crystals

MDPI

*Article*

# Theoretical Investigations of a BN Polymorph with $sp^2$ + $sp^3$ Hybridizations

**Xinhai Yu [1,2,*], Riguge Su [1,3], Bei He [1,3] and Binchang Ma [1,3]**

[1] Department of Mechanical and Electrical Engineering, Hetao College, Bayannur 015000, China; suriguge87@163.com (R.S.); hb12622455711@163.com (B.H.); mabinchang123@163.com (B.M.)
[2] CAAC Key Laboratory of Civil Aircraft Airworthiness Technology, Civil Aviation University of China, Tianjin 300300, China
[3] Research and Application Center of Automation, Hetao College, Bayannur 015000, China
* Correspondence: xhyu1987@163.com

**Abstract:** The crystal structure, mechanical anisotropy, elastic properties and electronic characteristics, as well as the stability, of *P*4/*m* BN are predicted by means of density functional theory. In this work, BN in the *P*4/*m* phase demonstrates mechanical and dynamical stability. Compared with the values of bulk *B*, *E* and *G* in the *P*4/*m* phase, the *B* of BN in the *P*4/*m* phase is greater than that of dz4 BN, while the *G* and *E* of *P*4/*m* BN are greater than those of *Pnc*2 BN and dz4 BN. The ratio of the bulk-to-shear modulus for *P*4/*m* BN is less than 1.75 and dz4 BN, dz2 BN and lzlz2 BN, indicating that *P*4/*m* BN is more brittle than dz4 BN, dz2 BN and lzlz2 BN. *P*4/*m* BN exhibits stronger mechanical anisotropy in *G* and *E* than *Pbca* BN, $P4_2/mnm$ BN and *Pm*-3*m* BN but much weaker mechanical anisotropy than *P*4/*mbm* BN, $B_7N_7$, $B_{11}N_{11}$ and $B_{15}N_{15}$. In addition, *P*4/*m* BN is a quasi-direct bandgap semiconductor, and the difference between the direct and the indirect bandgap is 0.008 eV. In order to obtain further characteristics of *P*4/*m* BN for future synthetic verification, the *X*-ray diffraction (XRD) patterns for *P*4/*m* BN are also calculated. Given its properties, *P*4/*m* BN is a good candidate for photoelectric devices.

**Keywords:** *P*4/*m* BN; mechanical anisotropy; electronic band structure; brittleness; *X*-ray diffraction



**Citation:** Yu, X.; Su, R.; He, B.; Ma, B. Theoretical Investigations of a BN Polymorph with $sp^2$ + $sp^3$ Hybridizations. *Crystals* **2021**, *11*, 1574. https://doi.org/10.3390/cryst11121574

Academic Editors: Alberto Girlando and Giuseppe Greco

Received: 9 November 2021
Accepted: 15 December 2021
Published: 16 December 2021



## 1. Introduction

As an isoelectronic structure in carbon materials, boron nitride has many polymorphs, such as $sp^3$ hybridizations [1–4], $sp^2$ hybridizations [5–8] and $sp^2$ + $sp^3$ hybridization BN [9], similar to carbon structures having many allotropes, including $sp^3$ hybridizations [10–14], $sp^2$ hybridizations [15–18] and $sp^2$ + $sp^3$ hybridizations [19–21]. Cubic boron nitride (c-BN) is potentially a third-generation semiconductor material with properties that make it suitable for electronic devices working under extreme circumstances, as well as deep UV luminescence emitters and detectors.

BN polymorphs are attracting increasing attention, not only because they have excellent wear resistance and are super hard, such as *Pbca*-BN [22], c-BN, P-BN [23], O-BN [24], BC8-BN [25], etc. A completely tetrahedral-bonded boron nitride within an orthorhombic system, namely *Pbca*-BN (space group: *Pbca*), was proposed by Zhang et al. [26] and investigated by Fan et al. using first-principles calculations [22]. According to Fan et al., the *B*, *G* and hardness of *Pbca*-BN are 344 GPa, 316 GPa and 60.1 GPa, respectively. Therefore, *Pbca*-BN presents super hard characteristics and may be used in important applications in technology and the industry. A novel polymorph of boron nitride with monoclinic symmetry, *m*-BN, was established by Ma et al. [27]. The *B*, *G*, *E* and hardness of *m*-BN are 329 GPa, 328 GPa, 729 GPa and 56.1 GPa, respectively, the bulk modulus of *m*-BN is slightly smaller than that of *Pbca*-BN and the *G* is slightly greater than that of *Pbca*-BN. BN polymorphs have attracted increased attention from researchers, because they are essentially broad-bandgap semiconductors, and they have excellent physical properties, such as

high thermal conductivity, great resistivity, high mobility, a small dielectric constant and strong breakdown electric field. They are recommended for the production of electronic equipment employed under extreme circumstances. Regarding *Pnma*-BN, the bandgap is 7.18 eV [28], which is larger than that of c-BN (6.1–6.4 eV [29,30]); thus, it may be the largest bandgap BN polymorph in theory. In contrast, the bandgaps of *Pbca*-BN, *m*-BN and *P*4/*mbm* BN are 5.399 eV, 4.629 eV and 4.8 eV [31], respectively. In addition to its super hard properties and wide bandgap, the BN polymorph has many other interesting properties, such as ductility in the case of $P2_13$ BN [32]. The $B/G$ ratio of $P2_13$ BN is 2.220, which is close to that of dz4-BN [6] and larger than that of lz2-BN [6], while it is lower than that of cT8-BN [5].

In this work, we propose an all $sp^2$ + $sp^3$ hybridization BN polymorph, *P*4/*m* BN, with dynamical stability and mechanical stability, and the physical characteristics (including crystal structure, mechanical anisotropy, elastic properties and electronic characteristics) of *P*4/*m* BN are analyzed by means of density functional theory [33,34].

## 2. Materials and Methods

As in the majority of crystal structure and physical characteristics predictions, the Perdew–Burke–Ernzerhof (PBE) functional of the exchange correlation potential and the generalized gradient approximation (GGA) [35] are used in this work, and the density functional theory (DFT) calculations are performed by utilizing the ultrasoft pseudopotentials [36] under the Cambridge Sequential Total Energy Package (CASTEP) code [37]. The valence electron structures of N and B are $2s^22p^3$ and $2s^22p^1$, respectively. A high *k*-point separation, smaller than or approximately equal to 0.025 $Å^{-1} \times 2\pi$, is used for *P*4/*m* BN, and $6 \times 6 \times 10$ Monkhorst-Pack meshes [38] are employed for a conventional cell of *P*4/*m* BN. The Broyden–Fletcher–Goldfarb–Shanno (BFGS) minimization scheme [39] is employed for crystal geometric majorization. The plane wave cut-off energy for structural majorization is 500 eV, and this was adopted for the crystal property calculations for *P*4/*m* BN. The electronic bands were investigated utilizing the Heyd–Scuseria–Ernzerhof (HSE06) hybrid functional [40]. All the phonon spectra of *P*4/*m* BN were investigated based on the density functional perturbation theory (DFPT) method [41].

## 3. Results and Discussion

### *3.1. Crystal Structure*

The crystal structures of the BN polymorphs are shown in Figure 1. The green and gray spheres represent B atoms and N atoms, respectively. According to Figure 1, in the crystal structure of *P*4/*m* BN, one conventional cell contains 12 N and 12 B atoms, and these N and B atoms are connected by $sp^2$ and $sp^3$ hybridizations, including eight nitrogen atoms and eight boron atoms connected by $sp^3$ hybridizations and four nitrogen atoms and four boron atoms connected by $sp^2$ hybridizations. The *P*4/*m* BN involves a 4-membered BN ring, 6-membered BN ring, 8-membered BN ring and 16-membered BN ring. These ring structures are composed of alternating connections of N atoms and B atoms, and there is only one 4-, 6- and 16-membered BN ring each, as well as two eight-membered rings. The lattice parameters of the crystal structures of *P*4/*m* BN are presented in Table 1, together with the lattice constants of other BN polymorphs. The theoretical results regarding the GGA level for c-BN are in better agreement with the experimental results [42] than those of the LDA method. Thus, the results presented later in this work are based on the GGA level. The volumes per BN unit of BN in the *P*4/*m*, *Pnc*2, dz4, dz2 and lzlz2 phases and c-BN are also shown in Table 1. All the BN polymorphs with $sp^2$ + $sp^3$ hybridizations and $sp^2$ hybridizations are larger than the $sp^3$ hybridizations (c-BN), so the bulk modulus of the BN polymorphs with $sp^2$ + $sp^3$ hybridizations and $sp^2$ hybridizations is less than that of c-BN.

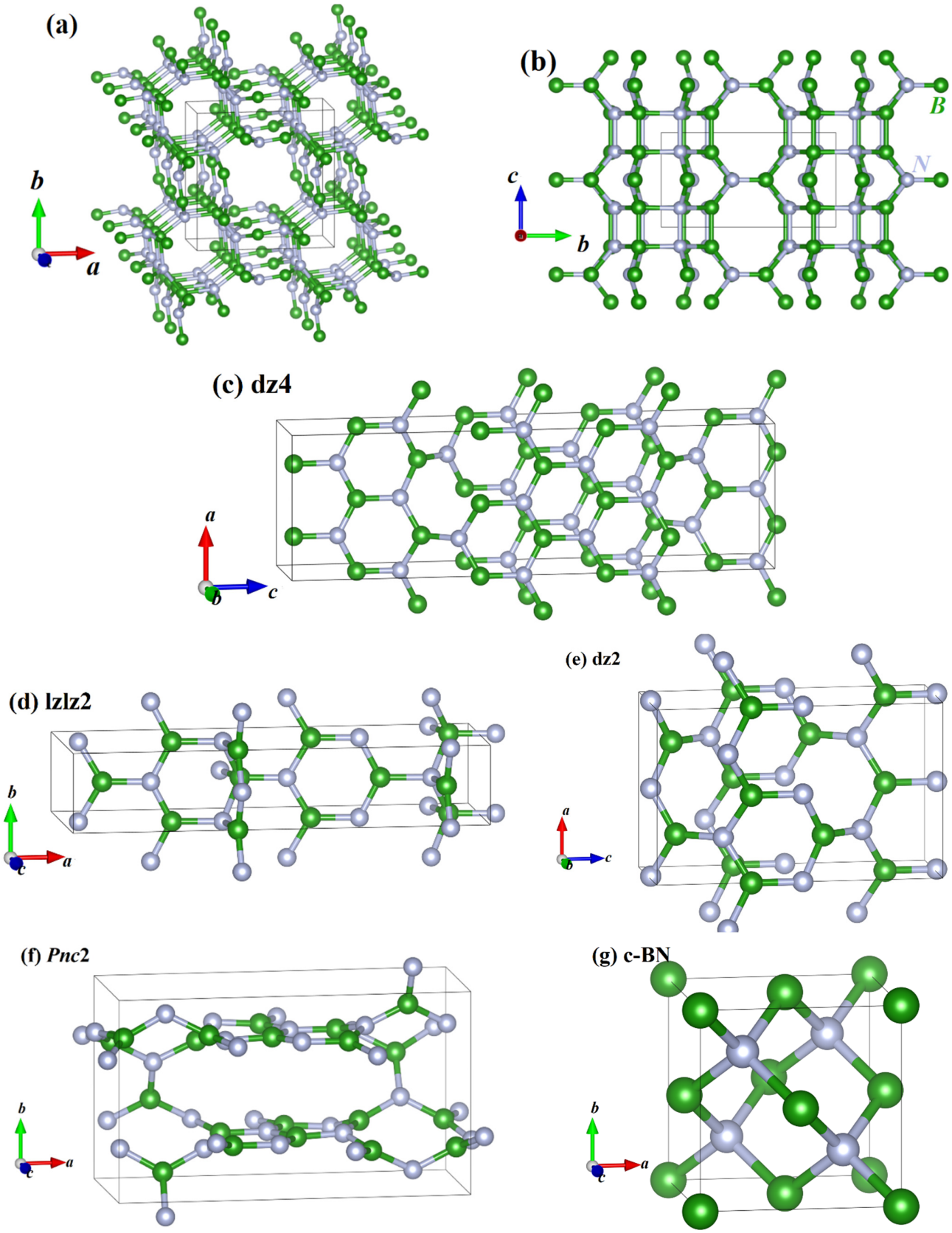


**Figure 1.** The crystal construction of *P*4/*m* BN (**a**), and the crystal construction of *P*4/*m* BN along the *a*-axis (**b**), dz4 BN (**c**), lzlz2 BN (**d**), dz2 BN (**e**), *Pnc*2 BN (**f**) and c-BN (**g**).

**Table 1.** Lattice constants (Å) and volumes per BN unit (Å$^3$) in the *P*4/*m*, *Pnc*2, dz4, dz2 and lzlz2 phases and c-BN.

| Materials | Methods | *a* | *b* | *c* | *β* | *V* | *ρ* |
|---|---|---|---|---|---|---|---|
| *P*4/*m* | GGA | 7.2455 | | 3.9257 | | 17.1740 | 2.3995 |
| | LDA | 7.1143 | | 3.8736 | | 16.3376 | 2.5334 |
| *Pnc*2 | GGA [1] | 10.9536 | 6.3020 | 4.9544 | | 17.1001 | 2.4099 |
| | LDA [1] | 10.8877 | 6.0603 | 4.9076 | | 16.1899 | 2.5454 |
| dz4 | GGA | 4.9850 | 3.4268 | 16.6081 | | 17.7321 | 2.3240 |
| dz2 | GGA | 4.9349 | 3.2640 | 8.0329 | | 16.1736 | 2.5480 |
| lzlz2 | GGA | 13.0946 | 2.5104 | 4.3953 | 89.3 | 18.0596 | 2.2819 |
| c-BN | GGA | 3.6217 | | | | 11.8762 | 3.4699 |
| | LDA | 3.5779 | | | | 11.4505 | 3.5989 |
| | Experimental [2] | 3.6200 | | | | 11.8595 | 3.4748 |

[1] Reference [9]. [2] Reference [42].

### 3.2. Stability

Stability is a significant physical property of new phases. In order to investigate the dynamical stability of *P*4/*m* BN, the phonon spectra of *P*4/*m* BN were generated, as presented in Figure 2. There was no hypothetical frequency observed in the entire Brillouin zone of *P*4/*m* BN, which proves that *P*4/*m* BN is dynamically stable. To study the mechanical stability of *P*4/*m* BN, the elastic constants of *P*4/*m* BN and other BN polymorphs were consulted, and these are shown in Table 2. The theoretical results of the elastic parameter $C_{ij}$ of c-BN are closer to the experimental results [43]; this also indicates that our prediction of the theoretical results of the elastic constants of *P*4/*m* BN is also reliable. The space group of *P*4/*m* BN is *P*4/*m*; it can be classified as having tetragonal symmetry, and the mechanical stability can be verified by [44]

$$C_{11} > 0, C_{33} > 0, C_{44} > 0, C_{66} > 0, \quad (1)$$

$$(C_{11} - C_{12}) > 0, (C_{11} + C_{33} - 2C_{13}) > 0, \quad (2)$$

$$[2(C_{11} + C_{12}) + C_{33} + 4C_{13}] > 0. \quad (3)$$

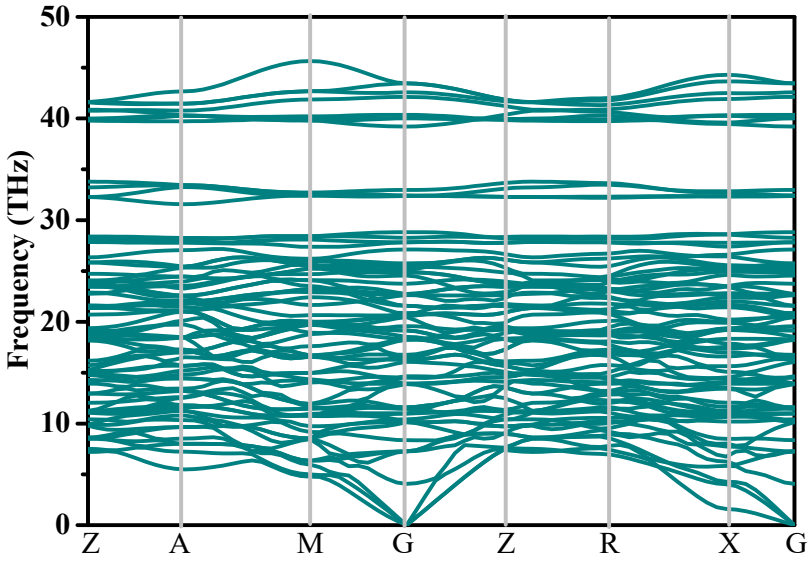


**Figure 2.** Phonon spectra of *P*4/*m* BN.

**Table 2.** The elastic parameters (GPa) and $E$ (Young's modulus), $B$ (bulk modulus) and $G$ (shear modulus) (GPa) of BN polymorphs with the GGA functional.

| Space Group | $C_{11}$ | $C_{22}$ | $C_{33}$ | $C_{44}$ | $C_{55}$ | $C_{66}$ | $C_{12}$ | $C_{13}$ | $C_{23}$ | $C_{16}$ | $C_{26}$ | B | G | E | B/G |
|---|---|---|---|---|---|---|---|---|---|---|---|---|---|---|---|
| P4/m | 261 | 261 | 539 | 138 | 138 | 69 | 90 | 65 | 65 | 3 | −3 | 160 | 117 | 282 | 1.368 |
| Pnc2 | 659 [1] | 122 | 661 | 36 | 136 | 56 | 117 | 149 | 68 | | | 176 | 93 | 237 | 1.892 |
| dz4 | 810 | 60 | 672 | 20 | 261 | 28 | 26 | 197 | 79 | | | 148 | 92 | 229 | 1.609 |
| dz2 | 786 | 107 | 629 | 86 | 290 | 72 | 64 | 229 | 131 | | | 183 | 127 | 309 | 1.441 |
| lzlz2 | 548 | 835 | 335 | 132 | 32 | 214 | 97 | 47 | 51 | | | 207 | 133 | 329 | 1.556 |
| c-BN | 779 | | | 447 | | | 165 | | | | | 370 | 384 | 856 | 0.964 |
| | 820 [2] | | | 480 | | | 190 | | | | | 400 | | | |

[1] Reference [9]. [2] Reference [43].

The elastic constants (see Table 2) of $P4/m$ BN satisfy the above Born criteria, thus proving that $P4/m$ BN are mechanically stable.

### *3.3. Mechanical and Mechanical Anisotropy Properties*

The elastic moduli and the $B/G$ of $P4/m$ BN are also shown in Table 2. The Voigt–Reuss-Hill approximations [45–47] are estimated for the values of $B$ and $G$. For the tetragonal structure, $B_V$, $B_R$, $G_V$ and $G_R$ can be taken as [48]

$$B_v = (1/9)[2(C_{11} + C_{12}) + C_{33} + 4C_{13}], \tag{4}$$

$$B_R = C^2/M, \tag{5}$$

$$C^2 = (C_{11} + C_{12})C_{33} - 2C_{13}^2. \tag{6}$$

$$M = C_{11} + C_{12} + 2C_{33} - 4C_{13}, \tag{7}$$

$$G_V = (1/30)(M + 3C_{11} - 3C_{12} + 12C_{44} + 6C_{66}), \tag{8}$$

$$G_R = 15\Big\{(18B_V/C^2) + [6/(C_{11} - C_{12})] + (6/C_{44}) + (3/C_{66})\Big\}^{-1}, \tag{9}$$

For the $B$, $G$ and $E$ of $P4/m$ BN, the following equations are used:

$$B = \frac{1}{2}(B_V + B_R), \tag{10}$$

$$G = \frac{1}{2}(G_V + G_R), \tag{11}$$

$$E = 9BG/(3B + G), \tag{12}$$

According to Table 2, the $B$ of the BN polymorphs with $sp^2$ + $sp^3$ hybridizations and $sp^2$ hybridizations, $P4/m$ BN, *Pnc*2 BN, dz4 BN, dz2 BN and lzlz2 BN, are all smaller than that of c-BN; this is consistent with our previous conclusions in the crystal structure section. In addition, the $B$ of $P4/m$ BN are greater than those of dz4 BN but less than those of *Pnc*2 BN, dz2 BN, lzlz2 BN and c-BN. In contrast, the $G$ and $E$ of $P4/m$ BN are greater than those of *Pnc*2 BN and dz4 BN and smaller than those of dz2 BN, lzlz2 BN and c-BN. The $B/G$ values of the BN materials are also shown in Table 2. It is well-known that $B/G < 1.75$ indicates ductility; otherwise, the material is brittle [49]. According to Table 2, the values for $P4/m$ BN, dz2 BN, dz4 BN, lzlz2 BN and c-BN are smaller than 1.75, i.e., their brittleness is confirmed; moreover, the $B/G$ of *Pnc*2 BN exceeds 1.75, which means that the ductility for *Pnc*2 BN is verified. Additionally, the ratio of the $B/G$ of $P4/m$ BN indicates its greater ductility compared to the other BN polymorphs mentioned in this work.

The mechanical anisotropy of crystals is very important in the study of their physical characteristics [50]. A directional dependence can visually show the anisotropic characteristics due to the varying Young's moduli generated in different planes. The three-dimensional (3D) surface is a regular sphere, which means that the material is isotropic; otherwise, the

material shows anisotropic characteristics [8,51–55], and the smaller the resemblance to a sphere, the larger the anisotropy, to evaluate the mechanical anisotropy properties of *E*.

For *P*4/*m* BN in distinct directions, the variations of *E* of *P*4/*m* BN in different planes were plotted, as shown in Figure 3a. In Figure 3a, different colors represent different value ranges: the minimum value and maximum value of *E* in *P*4/*m* BN are indicated by the curved surface of the solid cyan line and the solid purple line, respectively. The ratio between the maximum value and the minimum value ($E_{max}/E_{min}$ = 514.72/193.57 = 2.66) of *E* is greater than that of the *Pbca* phase [22], $P4_2/mnm$ phase [50] and *Pm*-3*m* phase [56], while it is much weaker than that of *P*4/*mbm* BN, $B_7N_7$, $B_{11}N_{11}$ and $B_{15}N_{15}$ [57]. The anisotropy in *E* of *P*4/*mbm* BN, $B_7N_7$, $B_{11}N_{11}$ and $B_{15}N_{15}$ is approximately 4, 6, 8 and 24 times that of *P*4/*m* BN, respectively. Therefore, the anisotropy in *E* of *P*4/*m* BN is much lower than that of *P*4/*mbm* BN, $B_7N_7$, $B_{11}N_{11}$ and $B_{15}N_{15}$. The two-dimensional (2D) extreme values of *E* in the (001), (101), (100), (110), (010) and (111) planes for *P*4/*m* BN are presented in Figure 3b, respectively. The distribution of *E* in the (100) plane and (010) plane is the same, including the $E_{max}$ and $E_{min}$, and the same situation also occurs in the (101) plane and (011) plane. The anisotropy in *E* of *P*4/*m* BN at the (001) plane ($E_{max}/E_{min}$ = 228.00/193.57 = 1.18) is the lowest, and the anisotropy in *E* at the (110) plane ($E_{max}/E_{min}$ = 514.72/194.54 = 2.65) is the strongest.

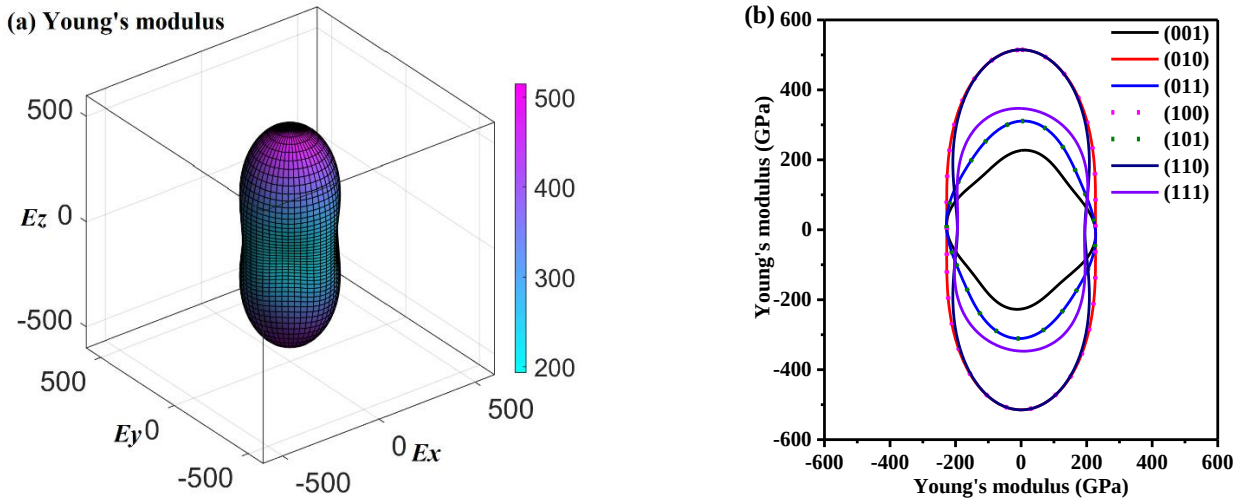


**Figure 3.** The directional dependence of the Young's modulus (in GPa) for *P*4/*m* BN, (**a**) and the 2D representation of Young's modulus (in GPa) for *P*4/*m* BN (**b**).

The variations of the $G_{max}$ and $G_{min}$ of *P*4/*m* BN in different directions are displayed in Figure 4a,b, which indicate the mechanical anisotropy properties of *G* for *P*4/*m* BN in distinct directions. The shape of the 3D-structured surface of *G* for *P*4/*m* BN is a very close sphere; the $G_{max}/G_{min}$ for *P*4/*m* BN is 2.08, while it is larger than that for the *Pbca* phase [22], $P4_2/mnm$ phase [50] and *Pm*-3*m* phase [56]. Regarding the Young's modulus, the anisotropy of the shear modulus of *P*4/*m* BN is still weaker than that of *P*4/*mbm* BN, $B_7N_7$, $B_{11}N_{11}$ and $B_{15}N_{15}$. The $G_{max}/G_{min}$ of *P*4/*mbm* BN, $B_7N_7$, $B_{11}N_{11}$ and $B_{15}N_{15}$ is still many times that of *P*4/*m* BN, and the anisotropy of *G* of *P*4/*mbm* BN, $B_7N_7$, $B_{11}N_{11}$ and $B_{15}N_{15}$ is approximately 7, 8, 14 and 44 times that of *P*4/*m* BN, respectively. The 2D representations of the shear modulus in the major planes for *P*4/*m* BN are provided in Figure 4c,d, respectively. As demonstrated in Figure 4c,d, as in the case of the Young's modulus, the distribution of *G* in the (100) and (010) planes is identical, and the distribution of *G* in the (101) plane and (011) plane is the same. The anisotropy of *G* of *P*4/*m* BN in the (110) plane ($G_{max}/G_{min}$ = 138.27/85.62 = 1.61) is the lowest, and the anisotropy of the shear modulus in the (101) and (011) planes ($G_{max}/G_{min}$ = 141.94/68.22 = 2.08) is the greatest.

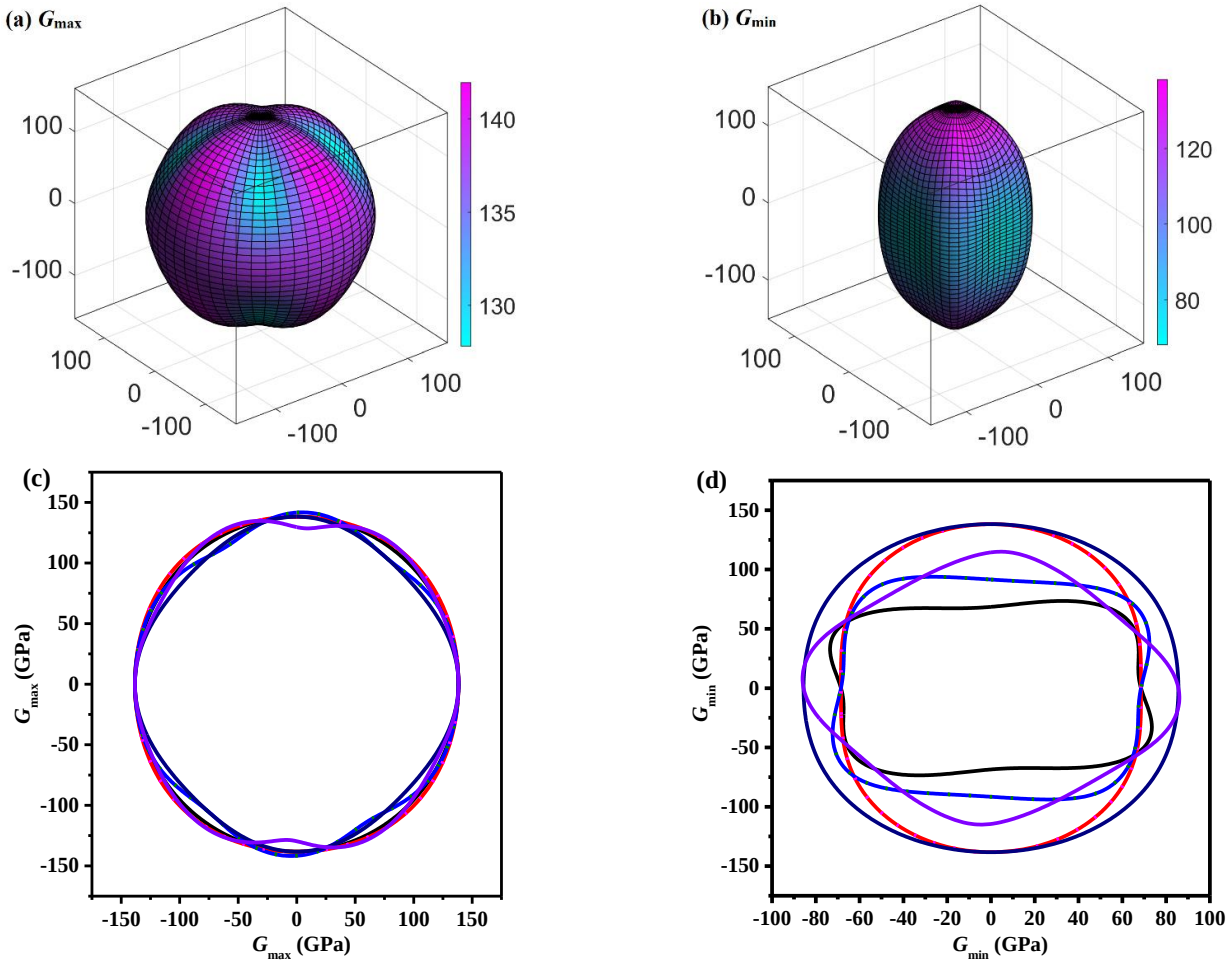


**Figure 4.** The directional dependence of the maximum values for the shear modulus (in GPa) for *P*4/*m* BN (**a**), the minimum values for the shear modulus (in GPa) for *P*4/*m* BN (**b**), the 2D representation of the maximum values for the shear modulus (in GPa) for *P*4/*m* BN (**c**) and the 2D representation of the minimum values for the shear modulus (in GPa) for *P*4/*m* BN (**d**).

The variations of the extremum value of $v$ for *P*4/*m* BN in different directions are demonstrated in Figure 5a,b, and the 2D representations of the Poisson's ratio in the (001), (101), (100), (110), (010) and (111) planes for *P*4/*m* BN are displayed in Figure 5c,d, respectively. The shape of the three-dimensional (3D) contour map of the *P*4/*m* BN shear modulus deviates far from the sphere; the $v_{max}/v_{min}$ for *P*4/*m* BN is 7.00, while it is larger than that of the *Pbca* phase [22], $P4_2/mnm$ phase [50] and *Pm*-3*m* phase [56]. Since all these materials are BN polymorphs, the reason for the differences in their anisotropy is not the different constituent elements. The anisotropy of the Young's modulus, Poisson's ratio and shear modulus is due to the different stacking modes of these BN polymorphs. Different stacking modes form different element rings. The larger the element ring, the larger the number of pore structures in these BN polymorphs. The more pore structures present, the greater the variations in the Young's modulus, shear modulus and Poisson's ratio in different directions. According to Figure 5c,d, for $E$ and the shear modulus, the distribution of $G$ in the (100) plane and (010) plane is the same, and the distribution of the Young's modulus and shear modulus in the (101) plane and (011) plane is the same. The anisotropy of the Poisson's ratio of *P*4/*m* BN in the (110) plane and (111) plane ($v_{max}/v_{min}$ = 0.42/0.06 = 7.00) is the largest, and the anisotropy in the $v$ ratio in the (100) and (010) planes ($v_{max}/v_{min}$ = 0.32/0.08 = 4.00) is the smallest.

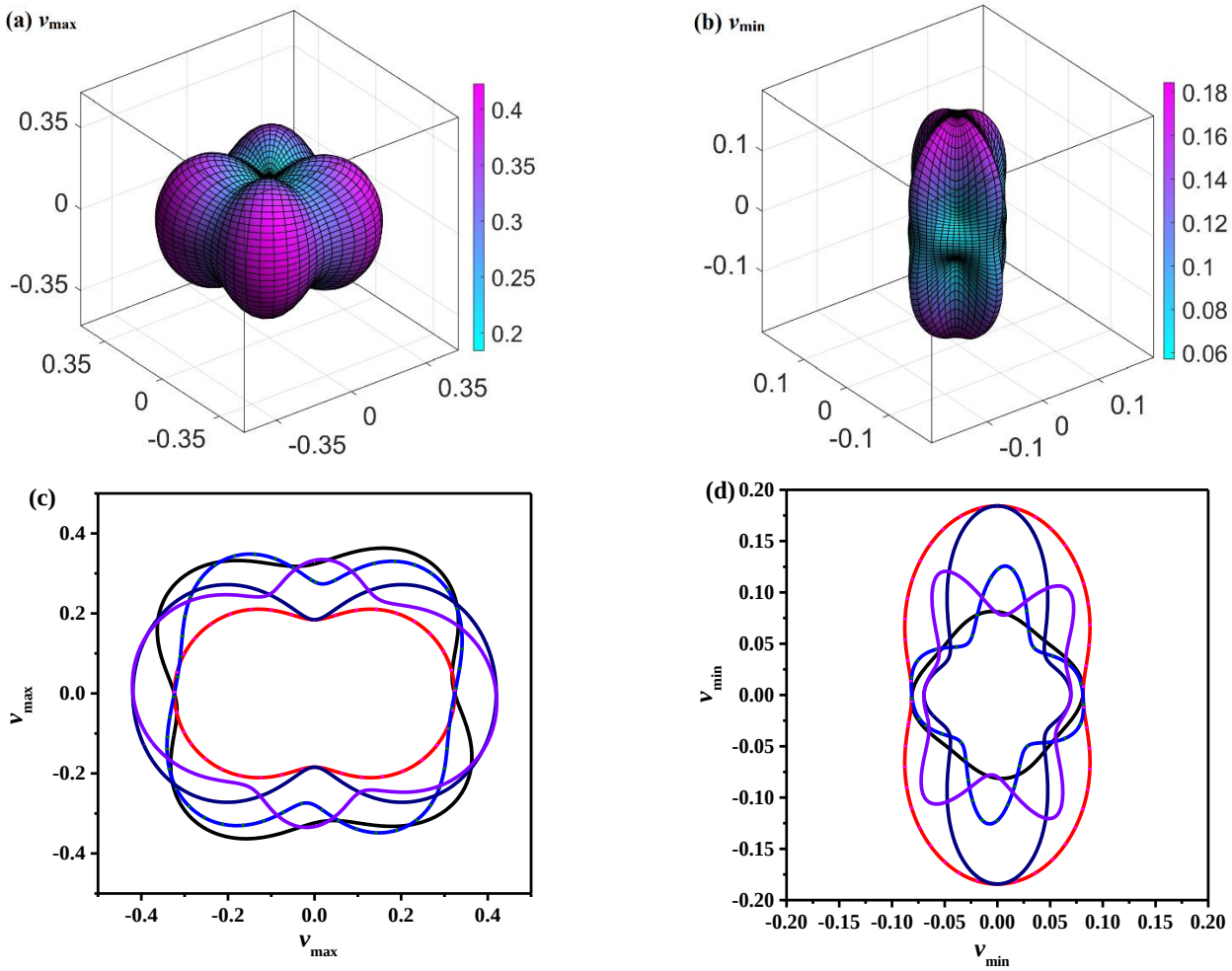


**Figure 5.** The directional dependence of the maximum values for Poisson's ratio for *P*4/*m* BN (**a**), the minimum values for Poisson's ratio for *P*4/*m* BN (**b**), the 2D representation of the maximum values for Poisson's ratio for *P*4/*m* BN (**c**) and the 2D representation of the minimum values for Poisson's ratio for *P*4/*m* BN (**d**).

### *3.4. Electronic Band Structures*

The electronic band structures and partial density of states (PDOS) using the HSE06 hybrid functional of *P*4/*m* BN and c-BN are plotted in Figure 6a,b, respectively. From Figure 6, one can observe that the *P*4/*m* BN is a semiconductor material with a quasi-direct bandgap, as it has a direct bandgap of 2.043 eV; while the direct bandgap of *P*4/*m* BN is 2.051 eV, the conduction band minimum (CBM) is located at the Z point, and the valence band maximum (VBM) is located at the A point. For other BN polymorphs, most of them are semiconductor materials and have a wide bandgap of more than 4 eV, such as $P4_2/mnm$ BN (6.13 eV [50]), *Pbca* BN (6.81 eV [22] and 6.79 eV [3]), *Pm*-3*m* BN (5.87 eV [56]), *m*-BN (4.629 eV [27]), *Pnma* BN (7.18 eV [28]), $B_4N_4$-II (5.32 eV [3]) and $B_4N_4$-I (4.86 eV [3]). Although the bandgap of *P*4/*m* BN is smaller than that of the above BN polymorphs, it is still larger than that of $P2_13$ BN (1.826 eV [32]). For *P*4/*m* BN, there are two hybridization modes of nitrogen atoms and boron atoms: $sp^2$ hybridization and $sp^3$ hybridization. The PDOS of atoms with different hybridization modes were studied, and the results are shown in Figure 6a. According to the partial density of the states in Figure 6a, the contribution of 2*p* orbitals from B atoms with $sp^2$ hybrids is larger than that of B atoms with $sp^3$ hybrids in the lower energy range (−8 to −4 eV), while the contribution of 2*p* orbitals from B atoms with $sp^2$ hybrids is less than that of B atoms with $sp^3$ hybrids in the range near the Fermi level (0 to 2 eV). For N atoms, the contribution from N 2*p* orbitals is greater than that of B 2*p* orbitals from 0 to 12 eV. In the range of 18–20 eV, the contribution of 2*p* orbitals

from N atoms with $sp^2$ hybrids is greater than that of N atoms with $sp^3$ hybrids, while the contribution of 2*p* orbitals from N atoms with $sp^2$ hybrids is less than that of N atoms with $sp^3$ hybrids at 15–18 eV and 20–22 eV. While, in c-BN, boron atoms and nitrogen atoms are all combined by $sp^3$ hybridization, in the energy range of −12 eV to the Fermi level, 6–20 eV, the contributions of the N 2*p* orbitals and B 2*p* orbitals are greater than those of the B 2*s* orbitals and N 2*s* orbitals; in the energy range from −22 eV to −15 eV, the contribution of B 2*p* orbitals is greater than that of B 2*s* orbitals, while the contribution of N 2*s* orbitals is greater than that of N 2*p* orbitals.

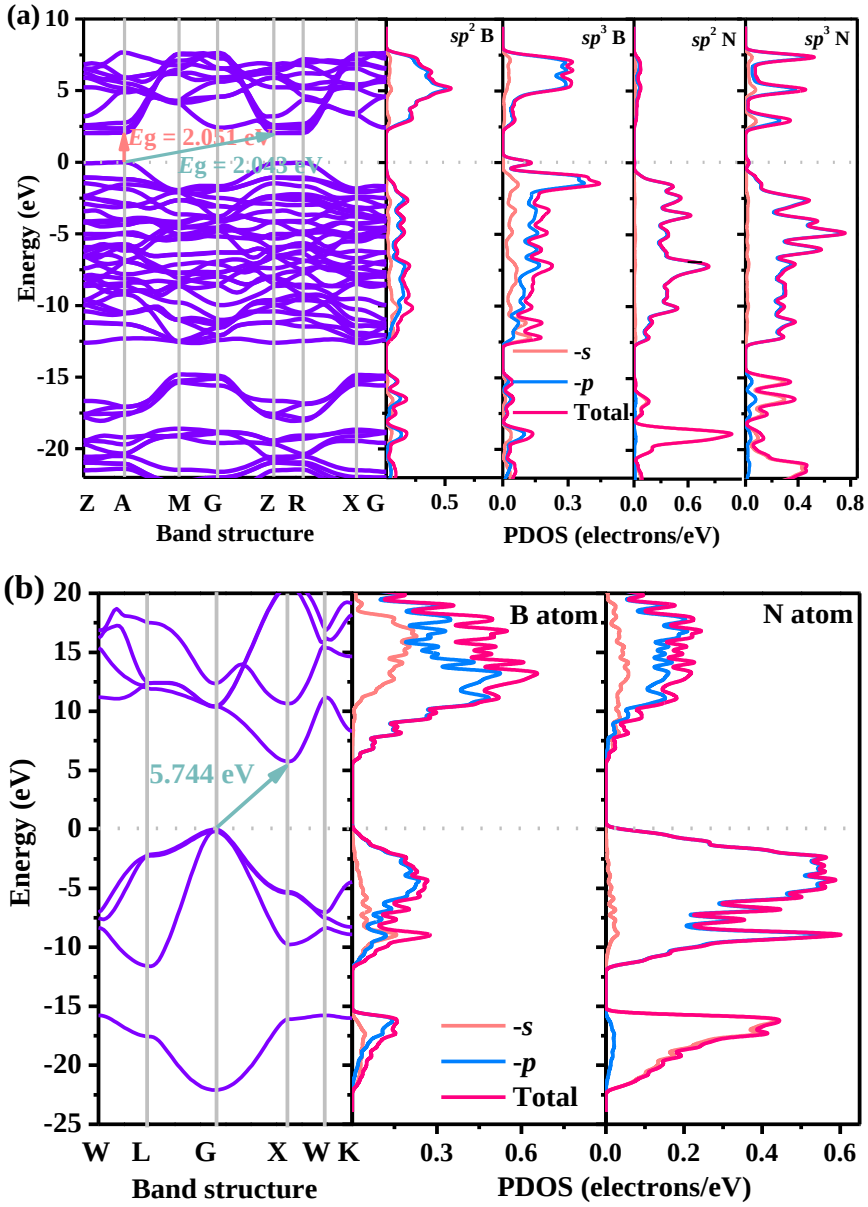


**Figure 6.** Electronic band structure and partial density of state for *P*4/*m* BN (**a**) and c-BN (**b**).

In addition, the electron localization functions (ELF) of *P*4/*m* BN and the band decomposed charge densities (BDCD) of *P*4/*m* BN are shown in Figure 7; the ELF with an isosurface level was set to 0.88, and the isosurface of the BDCD at the CBM and VBM was set to 0.005 eV/Å$^3$, respectively. The electron localization at the center of the $sp^3$ B–B bonds was stronger than that of the $sp^2$ + $sp^2$ BN bonds and stronger than that of the $sp^3$ − $sp^3$ BN bonds. The band decomposed charge densities (BDCD) of the CBM and VBM for *P*4/*m* BN are shown in Figure 7b,c, respectively. As shown in Figures 6 and 7b, the CBM is

composed mainly of $sp^3$ N 2*p* orbitals and $sp^2$ B atom 2*p* orbitals to a lesser extent, while the VBM is composed mainly of $sp^3$ B 2*p* orbitals and, to a lesser extent, $sp^3$ N atom 2*p* orbitals. Due to the quasi-direct bandgap of the *P*4/*m* BN, *P*4/*m* BN is a good candidate for photoelectric devices.

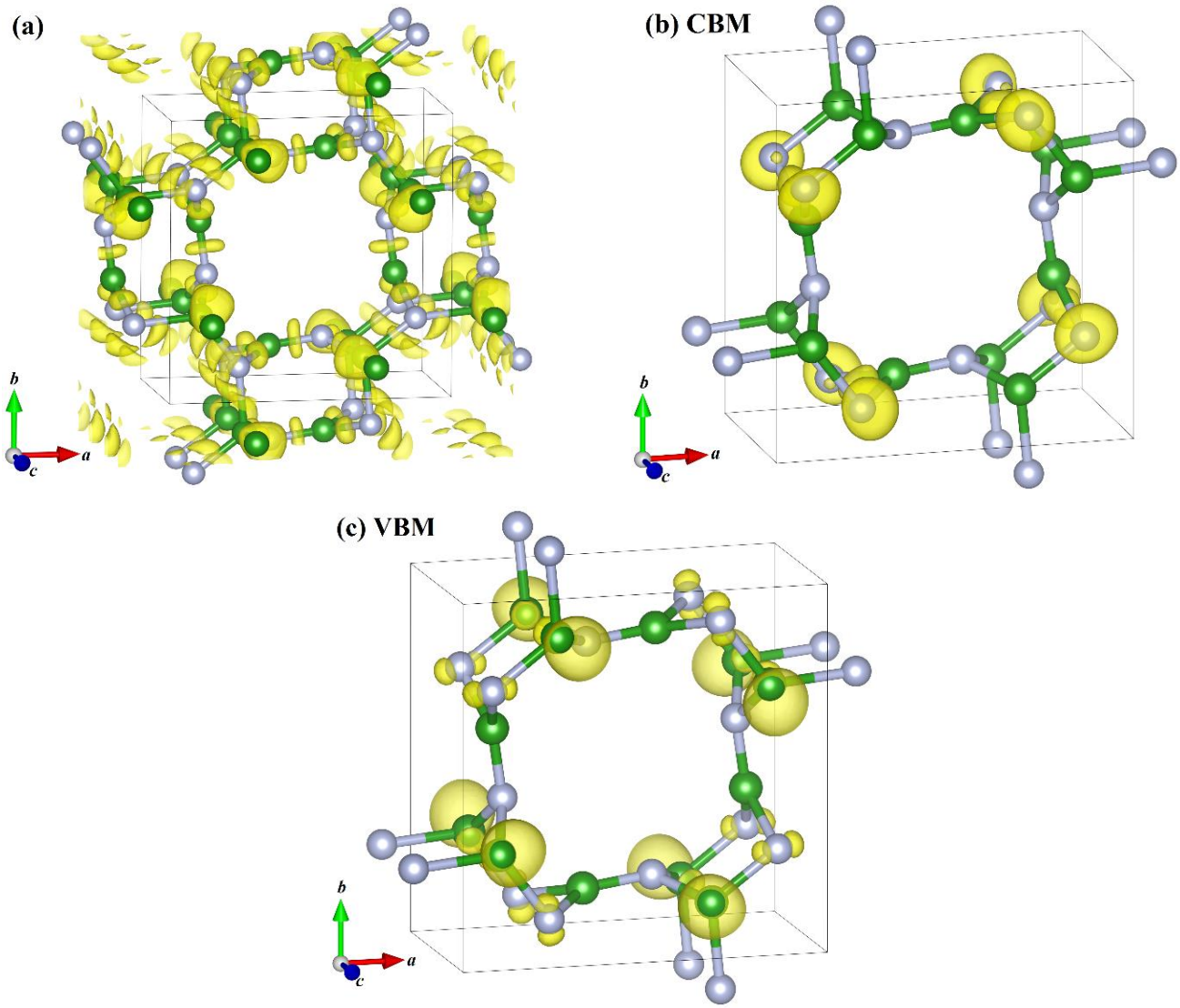


**Figure 7.** Electron localization functions with an isosurface level set to 0.88 (**a**), and band decomposed charge density (BDCD) for CBM (**b**) and VBM (**c**) of *P*4/*m* BN, the isosurface of the BDCD at the CBM and VBM was set to 0.005 eV/Å$^3$.

### *3.5. X-ray Diffraction*

In order to obtain further characteristics of *P*4/*m* BN for future synthetic verification, the simulation of *X*-ray diffraction (XRD) patterns for *P*4/*m* BN and other BN polymorphs was performed, as illustrated in Figure 8. Strong peaks of c-BN appeared between 40° and 90°, while strong peaks of *P*4/*m* BN appeared between 5° and 40°, respectively. The strongest peak of c-BN was (-1-1-1), which was located at around 43.21°, while the strongest peak of *P*4/*m* BN was (100), (110) and (200) for *P*4/*m* BN. In addition to the main diffraction peaks in Figure 7, the XRD spectrum also included several other weak diffraction peaks. For the (100) peak, the diffraction angles were 12.21° and 8.06° for *P*4/*m* BN and *Pnc*2 BN, respectively; for the (110) peak, the diffraction angles were 17.29°, 8.06° and 32.98° for *P*4/*m* BN, *Pnc*2 BN and dz2 BN, respectively. For the (011) peak, the diffraction angles were 22.81°, 29.62° and 26.79° for *Pnc*2 BN, dz2 BN and dz4 BN, respectively. For the (111)

peak, the diffraction angles were 28.62°, 24.23° and 32.34° for *P*4/*m* BN, *Pnc*2 BN and dz4 BN, respectively. These XRD characteristics are crucial for distinguishing the structures of *P*4/*m* BN in future experiments.

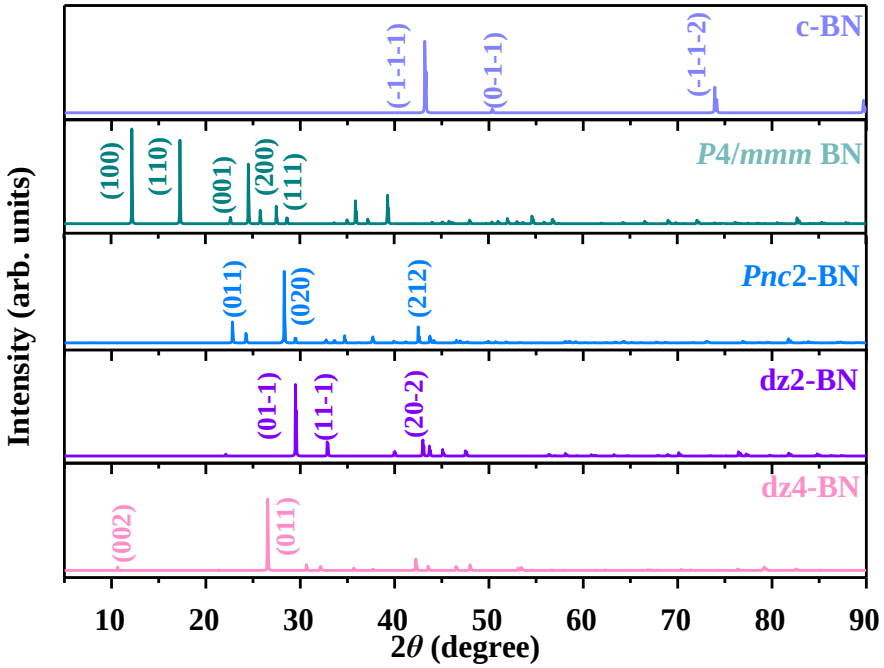


**Figure 8.** Simulated XRD patterns of *P*4/*m* BN using an *X*-ray wavelength (1.5406 Å) with a copper source.

## 4. Conclusions

In summary, three novel boron nitride polymorphs, *P*4/*m* BN, with wide bandgap properties are proposed theoretically through first-principles calculations. The structural characteristics, dynamical stability, mechanical stability, mechanical anisotropy, mechanical properties and electronic characteristics of *P*4/*m* BN are investigated in this work. *P*4/*m* BN has the strongest brittleness compared to that of dz2 BN, lzlz2 BN and dz4 BN. The *B* of *P*4/*m* BN is greater than that of dz4 BN but less than that of *Pnc*2 BN, dz2 BN, lzlz2 BN and c-BN. The *G* and *E* of *P*4/*m* BN are larger than those of *Pnc*2 BN and dz4 BN but smaller than those of dz2 BN, lzlz2 BN and c-BN. The anisotropy of the shear and Young's modulus of *P*4/*m* BN is greater than that of *Pbca* BN, $P4_2/mnm$ BN and *Pm*-3*m* BN, and it is less than that of *P*4/*mbm* BN, $B_7N_7$, $B_{11}N_{11}$ and $B_{15}N_{15}$. The $G_{max}/G_{min}$ and $E_{max}/E_{min}$ of *P*4/*mbm* BN, $B_7N_7$, $B_{11}N_{11}$ and $B_{15}N_{15}$ are still many times that of *P*4/*m* BN. In addition, *P*4/*m* BN is a quasi-direct and wide bandgap semiconductor material. *P*4/*m* BN may play an important role in the manufacture of photoelectric devices. Finally, it is possible that the XRD characteristics will be very helpful in determining the crystal structure of *P*4/*m* BN in future experiments.

**Author Contributions:** Methodology, X.Y.; investigation, X.Y., R.S., B.H. and B.M.; data curation, X.Y. and R.S.; writing—original draft preparation, X.Y.; project administration, X.Y. and R.S. and funding acquisition, X.Y. All authors have read and agreed to the published version of the manuscript.

**Funding:** This work was supported by the National Natural Science Foundation of China, grant number 61901162, the Research Project in Inner Mongolia Higher Education Institutions, grant number NJZY20222, and the Science and Technology Research Project of Hetao College, grant number HYZZ201930.

**Data Availability Statement:** Data are contained within the article.

**Acknowledgments:** Y. Liu (School of Microelectronics, Xidian University) is thanked for allowing us to use the CASTEP code in Materials Studio.

**Conflicts of Interest:** The authors declare no conflict of interest.

## References


1. Xiong, M.; Yuan, Z.; Mao, F.; Wang, X.; Jin, D.; Zhang, Q.; Yu, D.; Wang, C.; Wei, S. Superhard $B_{28}N_{32}$ with three-dimensional metallicity: First-principles prediction. *Comput. Mater. Sci.* **2021**, *188*, 110121. [CrossRef]
2. Tian, Y.; Kou, C.; Lu, M.; Yan, Y.; Zhang, D.; Li, W.; Cui, X.; Zhang, S.; Zhao, M.; Gao, L. Superhard monoclinic BN allotrope in M-carbon structure. *Phys. Lett. A* **2020**, *384*, 126518. [CrossRef]
3. Ma, Z.; Wang, P.; Yan, F.; Shi, C.; Tian, Y. Physical properties of B4N4-I and B4N4-II: First-principles study. *Chin. Phys. B* **2019**, *28*, 036101. [CrossRef]
4. He, C.; Sun, L.; Zhang, C.; Peng, X.; Zhang, K.; Zhong, J. Z-BN: A novel superhard boron nitride phase. *Phys. Chem. Chem. Phys.* **2012**, *14*, 10967–10971. [CrossRef]
5. Niu, C.; Wang, J. Three-dimensional three-connected tetragonal BN: Ab initio calculations. *Phys. Lett. A* **2014**, *378*, 2303–2307. [CrossRef]
6. Dai, J.; Wu, X.; Yang, J.; Zeng, X. Porous boron nitride with tunable pore size. *J. Phys. Chem. Lett.* **2014**, *5*, 393–398. [CrossRef]
7. Wang, H.; Zhang, W.; Huai, P. Novel 3D metallic boron nitride containing only $sp^2$ bonds. *J. Phys. D Appl. Phys.* **2017**, *50*, 385302. [CrossRef]
8. Ma, Z.; Zuo, J.; Wang, P.; Shi, C. Physical properties of Ima2-BN under pressure: First principles calculations. *Chin. J. Phys.* **2019**, *59*, 317–324. [CrossRef]
9. Yu, X.; Su, R.; He, B. A novel BN Polymorph with ductile manner. *J. Solid State Chem.* 2022, *in press*. [CrossRef]
10. Yang, X.; Lv, C.; Liu, S.; Zang, J.; Qin, J.; Du, M.; Yang, D.; Li, X.; Liu, B.; Shan, C. Orthorhombic C14 carbon: A novel superhard sp3 carbon allotrope. *Carbon* **2020**, *156*, 309–312. [CrossRef]
11. Fan, Q.; Peng, H.; Zhang, W.; Yu, X.; Yun, S. Physical properties of group 14 elements in *P*2/*m* phase. *J. Solid State Chem.* **2022**, *305*, 122641. [CrossRef]
12. Zhou, Y.; Chen, X.; Liu, S.; Gan, L. Three tetragonal superhard $sp^3$ carbon allotropes. *Solid State Commun.* **2021**, *323*, 114095. [CrossRef]
13. Li, S.; Zhang, J.; Wang, J.; Guan, S.; Li, Y. Dense as diamond: Pn-C10, a superhard $sp^3$ carbon allotrope. *Appl. Phys. Lett.* **2021**, *118*, 012107. [CrossRef]
14. Fan, Q.; Liu, H.; Jiang, L.; Yu, X.; Zhang, W.; Yun, S. Two orthorhombic superhard carbon allotropes: C16 and C24. *Diam. Relat. Mater.* **2021**, *116*, 108426. [CrossRef]
15. Fu, W.; Zhang, Y.; Shang, J.; Zeng, L.; Cai, Y. Lattice thermal conductivity and bandgap engineering of a three-dimensional sp2-hybridized Dirac carbon material: HS-C48. *Comput. Mater. Sci.* **2018**, *155*, 293–297. [CrossRef]
16. Su, H.; Lai, Z.; Kan, E.; Zhu, X. CP-C20, a new metallic cubic carbon allotrope with an $sp^2$ network. *J. Solid State Chem.* **2020**, *283*, 121136. [CrossRef]
17. Wang, Z.; Zhu, X.; Wang, M. A prediction of a new porous metallic carbon allotrope with an $sp^2$ hybridized network: cP-C24. *Solid State Sci.* **2020**, *105*, 106247. [CrossRef]
18. Zhao, C.; Yang, Y.; Niu, C.; Wang, J.; Jia, Y. C-57 carbon: A two-dimensional metallic carbon allotrope with pentagonal and heptagonal rings. *Comp. Mater. Sci.* **2019**, *160*, 115–119. [CrossRef]
19. Ram, B.; Mizuseki, H. C568: A new two-dimensional $sp^2$-$sp^3$ hybridized allotrope of carbon. *Carbon* **2020**, *158*, 827–835. [CrossRef]
20. Liu, L.; Hu, M.; Zhao, Z.; Pan, Y.; Dong, H. Superhard conductive orthorhombic carbon polymorphs. *Carbon* **2020**, *158*, 546–552. [CrossRef]
21. Fan, Q.; Liu, H.; Jiang, L.; Zhang, W.; Song, Y.; Wei, Q.; Yu, X.; Yun, S. Three-dimensional metallic carbon allotropes with superhardness. *Nanotech. Rev.* **2021**, *10*, 1266–1276. [CrossRef]
22. Fan, Q.; Wei, Q.; Yan, H.; Zhang, M.; Zhang, Z.; Zhang, J.; Zhang, D. Elastic and electronic properties of *Pbca*-BN: First-principles calculations. *Comput. Mater Sci.* **2014**, *85*, 80–87. [CrossRef]
23. Huang, Q.; Yu, D.; Zhao, Z.; Fu, S.; Xiong, M.; Wang, Q.; Gao, Y.; Luo, K.; He, J.; Tian, Y. First-principles study of O-BN: A $sp^3$-bonding boron nitride allotrope. *J. Appl. Phys.* **2012**, *112*, 053518. [CrossRef]
24. Jiang, X.; Zhao, J.; Ahuja, R. A novel superhard BN allotrope under cold compression of h-BN. *J. Phys-Condens. Mat.* **2013**, *25*, 122204. [CrossRef] [PubMed]
25. Ren, X.; Zhao, C.; Niu, C.; Wang, J.; Jia, Y.; Cho, J. First-principles study of the crystal structures and physical properties of H18-BN and Rh6-BN. *Phys. Lett. A* **2016**, *380*, 3891. [CrossRef]
26. Zhang, X.; Wang, Y.; Lv, J.; Zhu, C.; Li, Q.; Zhang, M.; Li, Q.; Ma, Y. First-principles structural design of superhard materials. *J. Chem. Phys.* **2013**, *138*, 114101. [CrossRef]
27. Ma, Z.; Zuo, J.; Tang, C.; Wang, P.; Shi, C. Physical properties of a novel phase of boron nitride and its potential applications. *Mater. Chem. Phys.* **2020**, *252*, 123245. [CrossRef]
28. Ma, Z.; Han, Z.; Liu, X.; Yu, X.; Wang, D.; Tian, Y. *Pnma*-BN: Another boron nitride polymorph with interesting physical properties. *Nanomaterials* **2017**, *7*, 3. [CrossRef] [PubMed]

29. Rodriguez-Hernandez, P.; Gonzales-Diaz, M.; Munoz, A. Electronic and structural properties of cubic BN and BP. *Phys. Rev. B* **1995**, *51*, 14705–14708. [CrossRef]
30. Ferhat, M.; Zaoui, A.; Certier, M.; Aourag, H. Electronic structure of BN, BP and Bas—The art of scientifique computing. *Phys. B* **1998**, *252*, 229–236. [CrossRef]
31. Zhao, M.; Chen, W.; Wu, W.; Li, B. A novel BN polymorph in *P*4/*mbm* phase with a (4,4) nanotube. *Phys. Status Solidi B* **2021**, 2100333. [CrossRef]
32. Fan, Q.; Wu, N.; Chen, S.; Jiang, L.; Zhang, W.; Yun, S. $P2_13$ BN: A novel large-cell boron nitride polymorph. *Commun. Theor. Phys.* **2021**, *73*, 125701. [CrossRef]
33. Hohenberg, P.; Kohn, W. Inhomogeneous electron gas. *Phys. Rev.* **1964**, *136*, B864. [CrossRef]
34. Kohn, W.; Sham, L. Self-consistent equations including exchange and correlation effects. *Phys. Rev.* **1965**, *140*, A1133. [CrossRef]
35. Perdew, J.; Burke, K.; Ernzerhof, M. Generalized gradient approximation made simple. *Phys. Rev. Lett.* **1996**, *77*, 3865. [CrossRef]
36. Vanderbilt, D. Soft self-consistent pseudopotentials in a generalized eigenvalue formalism. *Phys. Rev. B* **1990**, *41*, 7892R–7895R. [CrossRef]
37. Clark, S.; Segall, M.; Pickard, C.; Hasnip, P.; Probert, M.I.; Refson, K.; Payne, M. First principles methods using CASTEP. *Z. Kristallogr.* **2005**, *220*, 567–570. [CrossRef]
38. Monkhorst, H.J.; Pack, J.D. Special points for Brillouin-zone integrations. *Phys. Rev. B* **1976**, *13*, 5188–5192. [CrossRef]
39. Pfrommer, B.; Côté, M.; Louie, S.; Cohen, M. Relaxation of crystals with the Quasi-Newton method. *J. Comput. Phys.* **1997**, *131*, 233–240. [CrossRef]
40. Heyd, J.; Scuseria, G.; Ernzerhof, M. Hybrid functionals based on a screened Coulomb potential. *J. Chem. Phys.* **2003**, *118*, 8207–8215. [CrossRef]
41. Baroni, S.; de Gironcoli, S.; dal Corso, A.; Giannozzi, P. Phonons and related crystal properties from density-functional perturbation theory. *Rev. Mod. Phys.* **2001**, *73*, 515. [CrossRef]
42. Petrescu, M. Boron nitride theoretical hardness compared to carbon polymorphs. *Diam. Relat. Mater.* **2004**, *13*, 1848. [CrossRef]
43. Grimsditch, M.; Zouboulis, E.S.; Polian, A. Elastic constants of boron nitride. *J. Appl. Phys.* **1994**, *76*, 832. [CrossRef]
44. Mouhat, F.; Coudert, F.X. Necessary and sufficient elastic stability conditions in various crystal systems. *Phys. Rev. B* **2014**, *90*, 224104. [CrossRef]
45. Voigt, W. *Lehrburch der Kristallphysik*; Teubner, B.G., Ed.; Johnson Reprint Corp: Leipzig, Germany, 1928.
46. Reuss, A. Berechnung der Fließgrenze von Mischkristallen auf Grund der Plastizitätsbedingung für Einkristalle. *J. Appl. Math. Mech.* **1929**, *9*, 49–58. (In German) [CrossRef]
47. Hill, R. The elastic behaviour of a crystalline aggregate. *Phys. Soc. Lond. Sect. A* **1952**, *65*, 349. [CrossRef]
48. Wu, Z.; Zhao, E.; Xiang, H.; Hao, X.; Liu, X.; Meng, J. Crystal structures and elastic properties of superhard $IrN_2$ and $IrN_3$ from first principles. *Phys. Rev. B* **2007**, *76*, 054115. [CrossRef]
49. Pugh, S. XCII. Relations between the elastic moduli and the plastic properties of polycrystalline pure metals. *Lond. Edinb. Dublin Philosop. Mag. J. Sci. Ser.* **1954**, *45*, 823–843. [CrossRef]
50. Fan, Q.; Ai, X.; Zhou, J.; Yu, X.; Zhang, W.; Yun, S. Novel III-V nitride polymorphs in the $P4_2/mnm$ and *Pbca* phases. *Materials* **2020**, *13*, 3743. [CrossRef]
51. Duan, Y.; Sun, Y.; Peng, M.; Zhou, S. Anisotropic elastic properties of the Ca–Pb compounds. *J. Alloys Compd.* **2014**, *595*, 14–21. [CrossRef]
52. Fan, Q.; Hao, B.; Jiang, L.; Yu, X.; Zhang, W.; Song, Y.; Yun, S. Group 14 semiconductor alloys in the $P4_12_12$ phase: A comprehensive study. *Res. Phys.* **2021**, *25*, 104254. [CrossRef]
53. Qiao, L.; Jin, Z. Two B-C-O compounds: Structural, mechanical anisotropy and electronic properties under pressure. *Materials* **2017**, *10*, 1413. [CrossRef] [PubMed]
54. Fan, Q.; Liu, H.; Yang, R.; Yu, X.; Zhang, W.; Yun, S. An orthorhombic superhard carbon allotrope: *Pmma* $C_{24}$. *J. Solid State Chem.* **2021**, *300*, 122260. [CrossRef]
55. Fan, Q.; Li, C.; Yang, R.; Yu, X.; Zhang, W.; Yun, S. Stability, mechanical, anisotropic and electronic properties of oP8 carbon: A superhard carbon allotrope in orthorhombic phase. *J. Solid State Chem.* **2021**, *294*, 121894. [CrossRef]
56. Zhang, Q.; Zou, Y.; Fan, Q.; Yang, Y. Physical properties of XN (X = B, Al, Ga, In) in the *Pm*-3*n* phase: First-principles calculations. *Materials* **2020**, *13*, 1280. [CrossRef] [PubMed]
57. Zhang, S.; Wang, Q.; Kawazoe, Y.; Jena, P. Three-dimensional metallic boron nitride. *J. Am. Chem. Soc.* **2013**, *135*, 18216–18221. [CrossRef] [PubMed]